Kinetics and Mechanism of Steam Gasification of Char from Hydrothermally Treated Woody Biomass

Article *in* Energy & Fuels · November 2014

DOI: 10.1021/ef501898h

6 authors, including:

Lei Bai
West Virginia University
46 PUBLICATIONS **349** CITATIONS
SEE PROFILE

Karnowo Karnowo
9 PUBLICATIONS **60** CITATIONS
SEE PROFILE

Shinji Kudo
Kyushu University
80 PUBLICATIONS **900** CITATIONS
SEE PROFILE

Koyo Norinaga
Kyushu University
127 PUBLICATIONS **2,496** CITATIONS
SEE PROFILE

energy&fuels

Article

pubs.acs.org/EF

Kinetics and Mechanism of Steam Gasification of Char from Hydrothermally Treated Woody Biomass

Lei Bai,[†,‡] Karnowo,[†] Shinji Kudo,[†] Koyo Norinaga,[†] Yong-gang Wang,[‡] and Jun-ichiro Hayashi*[,†]

[†]Institute for Materials Chemistry and Engineering, Kyushu University, 6-1, Kasuga Koen, Kasuga 861-8580, Japan

[‡]Department of Chemical Engineering and Technology, School of Chemical and Environmental Engineering, China University of Mining and Technology, Beijing (CUMTB), Beijing 100083, People's Republic of China

ABSTRACT: Hydrothermal treatment (HTT) is a promising way of upgrading biomass as a solid fuel and precursor of carbon materials by eliminating or transforming carbohydrates and also leaching alkali and alkaline earth metallic (AAEM) species. This study investigated steam gasification of a woody biomass that had been upgraded by HTT at 250 °C. HTT removed 87−97% of AAEM species from the biomass. The char from the pyrolysis of the treated biomass underwent gasification, obeying first-order kinetics with respect to the mass of char over the entire range of conversion. This kinetics arose from non-catalytic gasification. AAEM species remaining in the char had no catalytic activity. The specific surface area of char increased monotonically with its conversion from 500 to well above 2000 m^2/g. The non-catalytic nature of the gasification was responsible for such a significant surface area development. The surface area was, however, not a factor influencing the rate of gasification. The presence of the inherent AAEM catalyst and that of the extraneous potassium catalyst altered the kinetics of gasification to zeroth order while suppressing the surface-area development not only creating but also consuming micropores. The surface area was not a kinetic factor for the catalytic gasification.

1. INTRODUCTION

Hydrothermal treatment (HTT) is a heat treatment in hot-compressed water (HCW) well above 100 °C and is a promising way to pretreat lignocellulosic biomass. Hydrolytic decomposition of carbohydrates (i.e., cellulose and hemicellulose)[1−5] has long been studied, because it forms sugar monomers and oligomers that are essential for producing ethanol, methane, or acids by fermentation. The saccharides can be further converted in HCW to chemicals,[6−11] such as acids (e.g., acetic, formic, and levulinic acids), furans (furfural and 5-hydroxymethyl furfural), and aromatics (xylenes and phenols). HTT also hydrolyzes lignin, but it seems to be difficult to recover phenolic compounds as monomers at substantial yield, because retrogressive reactions are predominant in HCW.[12,13] HTT is also effective for upgrading the biomass to a solid fuel with a much higher calorific value and lower moisture content than the original.[14−16] These properties are caused mainly by the removal of oxygen-rich carbohydrates. Thus, HTT has potential to produce upgraded solid fuel together with water-soluble sugars or other chemicals.

A recently proposed application of HTT is the production of lignin-rich solid and its conversion to metallurgical coke.[17] The hydrothermal treatment around 250 °C produced a solid that consisted of lignin and non-hydrolyzable material derived from the carbohydrates. The solid was successfully converted to coke with a tensile strength of 40−50 MPa, which was higher by 8−10 times that of general commercial coke, by a sequence of hot briquetting and carbonization.[18] Such high mechanical strength was attributed to the removal and chemical transformation of the carbohydrates, of which a highly volatile nature inhibited the formation of coke with a high density.

It is expected from a viewpoint of solid fuel or material production that HTT has another feature, that is, removal of metallic species. During HTT, the water phase becomes acidic because of the formation of acids.[9−11] It is then suggested that HTT can remove the alkali and alkaline earth metallic (AAEM) species from the biomass. The pH of the water resulting from HTT is around 3.0 or lower, which is low enough to remove major portions of mono- and divalent cations.[18] The removal of AAEM species enables the avoidance of ash problems in the subsequent combustion or gasification and also controls the reactivity of metallurgical coke within an appropriate range of coke reactivity index (CRI) by removing AAEM species that catalyze CO_2 gasification of the coke.

In gasification of biomass, AAEM species are often responsible for ash problems, such as slugging and defluidization in the gasifier, and erosion/corrosion of material in the downstream.[19−25] Such problems can be avoided by HTT. On the other hand, the removal of AAEM species, in other words, the major catalytic species, will considerably change the characteristics of gasification of char[26−29] and reforming of volatiles over the char.[30,31] The gasification of char from the pyrolysis of biomass is contributed by non-catalytic gasification and AAEM-catalyzed gasification.[29] These two modes of gasification differ clearly from each other regarding the rate of reaction and its variation with the progress of char conversion. It is thus expected that HTT greatly changes the characteristics of gasification of char from the biomass.

The present authors[32] prepared chars from the pyrolysis of seven different types of biomass, removed AAEM species from the chars by acid washing, and investigated non-catalytic steam gasification of them. It was found that all of the chars

Received: August 25, 2014
Revised: October 8, 2014
Published: October 9, 2014

   dx.doi.org/10.1021/ef501898h | *Energy Fuels* 2014, 28, 7133−7139

underwent gasification obeying first-order kinetics with respect to the mass of char, during which the specific rate of gasification

$$r_{sp} = \frac{dX}{dt(1-X)} \quad (X = \text{conversion of char}) \tag{1}$$

was maintained steady over the entire range of char conversion. Thus, despite a gas−solid reaction, the non-catalytic steam gasification was recognized as a homogeneous gasification. On the other hand, the specific surface areas of the chars increased monotonically from ca. 500 to 2700 m^2/g. The considerable development of the surface area suggested application of AAEM-species-free char for production of high-performance and clean active carbon.

The present study investigated a sequence of HTT, pyrolysis, and steam gasification of a typical woody biomass with the primary purpose to examine the first-order kinetics of the steam gasification and characteristics of surface area development. The secondary purpose was to examine roles played by inherent AAEM species and extraneous (i.e., intentionally added) species in the kinetics and surface area development and further discuss a longstanding issue on the relationship between the rate of gasification and surface area of char, together with the effect of catalysis on the pore development.[33−45]

2. EXPERIMENTAL SECTION

2.1. HTT of Biomass. Sawdust of a Japanese cedar (*Cryptomeria japonica*) with particle sizes ranging from 40 to 850 μm was dried at 110 °C to a moisture content below 2 wt % dry cedar and stored in a desiccator until use. The HTT and post-treatments were performed according to the procedure described below. A 15 g portion of the cedar was charged into a 250 mL autoclave together with 105 mL of deionized water (electroresistance > 18.2 MΩ). The autoclave was closed, pressurized with N_2 (purity > 99.9996 vol %) to 1.0 MPa, and then heated in a fluidized sand bath at 250 °C. This temperature was chosen because it was high enough to convert a major portion of the carbohydrate and sufficiently low to avoid carbonization of the lignin in woody and herbaceous biomass.[17] After heating for 60 min, the autoclave was transferred to an iced water bath and quenched. The entire portion of the solid/liquid suspension was taken out of the autoclave and separated by vacuum filtration into the solid and liquid. The solid was washed with 20 mL of deionized water under ultrasonication for 10 min, separated from the water in the same way as above, and then vacuum-dried at 60 °C for 24 h. The solid thus prepared is hereafter referred to as cedar HTT. Repeated runs of HTT confirmed the reproducibility of the yield (57 wt % dry cedar) and elemental composition of the cedar HTT.

2.2. Pyrolysis for Char Preparation. Five different char samples, char I, char II, char IIa, char IIa-K1, and char IIa-K2, were prepared. Figure 1 is a flowchart for the preparation of these char samples. Char I was prepared by the pyrolysis of the original cedar in a horizontal quartz tube reactor with a heating rate, peak temperature, and holding time of 10 °C/min, 900 °C, and 0 min, respectively. The cedar was heated under atmospheric flow of N_2 (purity, >99.9996 vol %; flow rate, 0.3 L_N/min). The other chars were prepared in a partial or full sequence of HTT, pyrolysis, acid washing, and impregnation of K_2CO_3. Char II was prepared from the pyrolysis of cedar HTT. Char IIa was prepared from the acid washing of char II. The acid washing employed the following conditions: acid reagent, 3 N HCl aqueous; washing time and temperature, 8 h and 60 °C, respectively. The acid-washed char IIa was washed with deionized water exhaustively until the absence of chlorine ion and vacuum-dried at 60 °C for 24 h. Char IIa was also loaded with potassium by a wet impregnation of K_2CO_3. A prescribed amount of char IIa was mixed with an aqueous solution of K_2CO_3 at 55 °C for 1 h, and the water was removed from the suspension in a rotary evaporator. The K_2CO_3-impregnated chars, char IIa-K1 and char IIa-K2, with K contents of 0.95 and 4.62 wt % dry

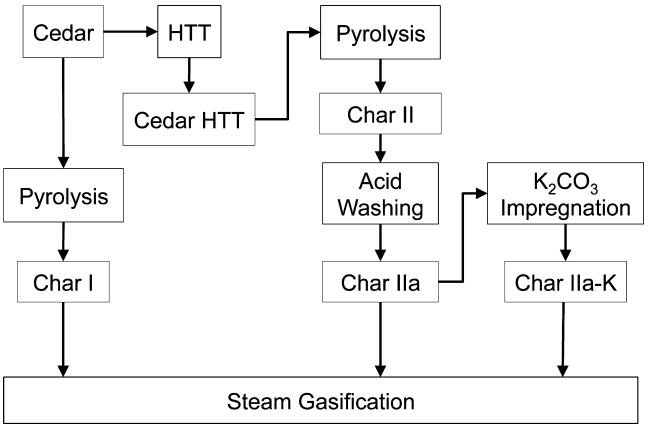

Figure 1. Process sequences for the preparation of char samples.

char IIa, respectively, were thus prepared. Table 1 shows properties of the cedar, cedar HTT, and chars. The chars thus prepared from HTT and pyrolysis were crushed and sieved to obtain particles below 75 μm and then subjected to the following analyses.

2.3. Quantification of AAEM Species. The contents of AAEM species in the cedar, cedar HTT, and chars were determined following a procedure reported elsewhere.[46] In brief, 10 mg of the solid was placed in a platinum crucible and then heated to 600 °C in a flow of air. The heating rate was as low as 1 °C/min for avoiding the ignition of the solid. The solid remaining in the crucible, i.e., the ash, was dissolved in a mixture of concentrated aqueous solutions of HF/HNO_3 (1:1, by mole) at 60 °C for 24 h. The acids were then evaporated, and the residue was redissolved in an aqueous solution of 0.04 N methanesulfonic acid. The solution was analyzed by ion chromatography for quantification of AAEM species. Their contents are shown in Table 1.

2.4. Steam Gasification of Char. The steam gasification was performed in a thermogravimetric analyzer (EXSTAR TG/TGA 6200, SII Nanotechnology, Inc.) that was equipped with a steam generator and its interface with the furnace tube.[32] The char sample with a mass of 1−2 mg was placed in a platinum crucible (5.2 mm in diameter and 2.5 mm in depth), set in the furnace tube, and heated at a rate of 30 °C/min up to 850 °C in an atmospheric flow of N_2 (flow rate, 0.70 L_N/min). Then, the N_2 flow was switched to that of a steam/N_2 mixture (20:80, vol/vol) without changing the volumetric flow rate. After confirmation that the gasification was near complete, the flowing gas was switched to air for the complete removal of the carbonaceous part of the char and determination of the mass of the ash. The mass-based conversion of the char by the steam gasification was determined as a function of time by the following equation:

$$X = 1 - \frac{m - m_{ash}}{m_0 - m_{ash}} \tag{2}$$

where m_0, m, and m_{ash} are masses of char at the beginning of gasification (t = 0), char at time t, and ash, respectively.

2.5. Measurement of the Surface Area of Char. The chars were also subjected to steam gasification in another horizontal furnace. The char with a mass of 0.07−0.08 g was placed in a quartz-made boat, placed within the isothermal section of the furnace, and heated in an atmospheric flow of N_2 (flow rate, 0.7 L_N/min) to 850 °C, where the gas flow was switched to mixed gases of steam and N_2 (20:80, vol/vol) at the same flow rate. The mixed gases were fed for a limited period, so that the gasification was terminated at a certain conversion of char. Partially gasified char samples with different conversions were thus prepared from char II, char IIa, char IIa-K1, and char IIa-K2. The partially gasified char IIa-K1 and char IIa-K2 were washed with water for removal of potassium species, dried, and then subjected to the surface area measurements.

The specific surface area of the char was measured with a NOVA 3200e, Quantachrome. The Brunauer−Emmett−Teller (BET) surface area, S_{BET}, was determined from the N_2 adsorption isotherm at −196

dx.doi.org/10.1021/ef501898h | Energy Fuels 2014, 28, 7133−7139

Table 1. Ash Contents and Elemental Compositions of Solids

solid	cedar	cedar HHT	char I	char II	char IIa	char IIa-K1	char IIa-K2
			wt % on a Dry Basis				
ash	3.5	1.3	nd	0.8	0.9	1.6	9.1
			wt % on a Dry and Ash-Free Basis				
C	49.9	64.8	nd	94.6	88.2	92.5	82.3
H	6.0	5.5	nd	0.6	0.5	0.6	0.8
N	0.1	0.2	nd	0.3	0.3	0.4	0.5
			wt % on a Dry Basis				
K	0.17	0.04	0.67	0.05	0.01	0.95	4.62
Na	0.04	<0.01	0.05	<0.01	<0.01	<0.01	<0.01
Mg	0.17	<0.01	0.17	0.01	0.01	0.02	0.01
Ca	0.14	0.11	0.78	0.19	0.06	0.19	0.13

°C and relative pressure (p/p_0) lower than 0.05. Another type of surface area, S_{CO_2}, was determined by analyzing the CO_2 adsorption isotherm at 0 °C based on a non-localized density functional theory (NLDFT) that was available in data reduction software by Quantachrome. S_{CO_2} was the specific surface area that has arisen from the pores having widths of 0.35−1.5 nm. On the other hand, the smallest pore size measurable by N_2 adsorption is around 0.5 nm.[32] More details of the analysis of the porous structure of char are available elsewhere.[32]

3. RESULTS AND DISCUSSION

3.1. Characteristics of Gasification of Char II and Char IIa. The net removal rates of K, Mg, and Ca by HTT, which were calculated by the following equation, were 87, 97, and 92%, respectively:

$$\text{removal rate} = 1 - ((C_{AAEM,HTT}, \text{wt \% dry cedar HTT})(Y_{s,HTT}, \text{wt \% dry cedar})/(C_{AAEM,cedar}, \text{wt \% dry cedar})) \quad (3)$$

where $C_{AAEM,cedar}$ and $C_{AAEM,HTT}$ are the contents of AAEM species in the cedar and cedar HTT on the respective dry mass bases. $Y_{s,HTT}$ is the mass yield of cedar HTT. The removal rate of Na was not determined accurately because of contamination of the liquid from HTT from a laboratory glass apparatus, but it was believed to be as high as that of K. Thus, a major portion of AAEM species was removed from the cedar by HTT, which acidified the water to pH of 2.9−3.0 by forming organic acids. The acid washing (AW) further decreased the K and Ca contents in char I from 0.05 to 0.01 wt % and from 0.19 to 0.06 wt %, respectively (see Table 1).

Figure 2 shows the time-dependent changes in X for char II and char IIa during the steam gasification. The kinetics for these chars are near identical to each other. There was thus no or very little effect of the acid washing on the kinetics. The acid washing removed major portions of K and Ca that had been retained by char II, and the acid-soluble species had no or negligible catalytic activities. It is noted that $\ln(1 - X)$ decreases linearly with t at $(1 - X) \leq 0.42$ (blue line in Figure 2), where the gasification took place obeying first-order kinetics, i.e.

$$\frac{dX}{dt} = k_{app,first}(1 - X) \quad (4)$$

where $k_{app,first}$ is the apparent rate constant and is steady at $(1 - X) \leq$ ca. 0.42. This first-order kinetics is indicative of progress of homogeneous gasification of the char as a single reacting component at $(1 - X) \leq$ ca. 0.42. Previous studies[29,32,47,48]

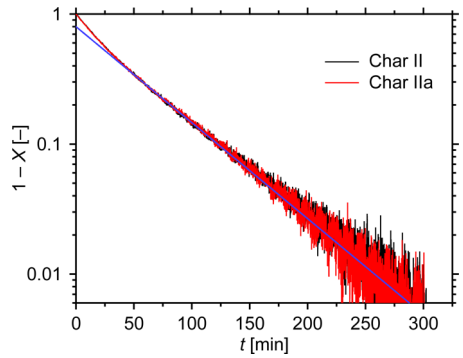

Figure 2. Plots of $(1 - X)$ on the logarithmic scale against t for the steam gasification of char II and char IIa.

claimed that chars from the acid-washed lignite or biomass underwent non-catalytic gasification with first-order kinetics over the entire range of char conversion. Then, it was strongly suggested that the gasification of char II and char IIa, at least within the range of $X \geq 0.58$, was non-catalytic gasification and that the acid-insoluble AAEM species (K, 0.01 wt %; Ca, 0.06 wt %) had no or very little catalytic activities. In other words, HTT had fully removed the catalyst precursors. Further discussion will be made on the kinetics of the gasification of char II and char IIa.

Figure 3 shows the changes in S_{BET} of char II and char IIa with X. There are two important trends. First, S_{BET} of char IIa agrees well with that of char II. The acid-soluble AAEM species, which had no catalytic activities, hardly influenced the surface area development of the char during the gasification. Second, both S_{BET} values increase monotonically and in a linear manner

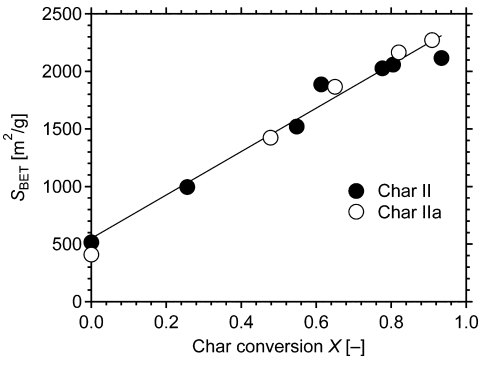

Figure 3. Changes in S_{BET} with the progress of gasification of char II and char IIa.

dx.doi.org/10.1021/ef501898h | Energy Fuels 2014, 28, 7133−7139

with X. S_{BET} at $X = 0.9$ is as high as 2300 m^2/g. This trend is in good agreement with those for the steam gasification of acid-washed biomass chars.[32]

The analysis of the $(1 - X)$ versus t relationships in Figure 2 by eq 4 shows that $k_{app,first}$ decreases gradually with X until it reaches ca. 0.58 and then becomes steady. It was thus difficult to correlate the rates of gasification of char II and char IIa with their S_{BET} values. The relationship between the rate of gasification and S_{BET} will be discussed later in more detail.

3.2. Kinetic Analysis of Gasification of Char I. Figure 4 shows $(1 - X)$ on a decimal scale for the gasification of char I

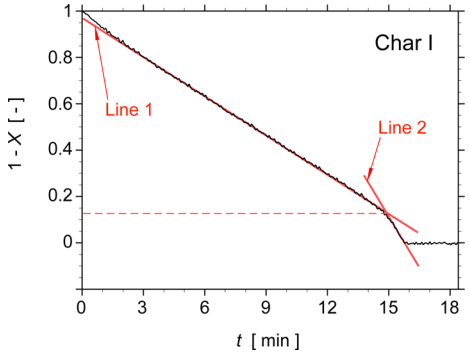

Figure 4. $(1 - X)$ for the gasification of char I as a function of t. Slopes of the lines 1 and 2 correspond to $k_{app,zeroth}$ at $X < 0.87$ and $X > 0.87$, respectively.

as a function of t. The rate of gasification of char I is much greater than those of char II and char IIa. This is attributed to the catalysis of the inherent AAEM species, the major portions of which were removed by HTT. X increases with t in a linear manner over a range up to 0.87. Such zeroth-order kinetics is attributed to the catalysis of AAEM species.[29,47,48]

$$\frac{dX}{dt} = k_{app,zeroth} \tag{5}$$

The zeroth-order kinetics indicates that not the concentration but the amount of active catalysts determined the rate of gasification. This indication is valid with a high degree of dispersion of the catalysts in the carbonaceous matrix and maintenance of the dispersion. It is also noted that the apparent rate constant, $k_{app,zeroth}$, increases suddenly around $X \approx 0.87$. Such a change in $k_{app,zeroth}$ can be explained by the catalyst concentration reaching a critical level, which is often termed the loading saturation level (LSL).[49−52] The saturation causes the highly dispersed catalysts to grow to more active clusters. The progress of gasification with steady and increasing $k_{app,zeroth}$ at $X < 0.87$ and $X > 0.87$, respectively, is indicative of no or insignificant deactivation of the catalysts.

3.3. Kinetic Analysis of Gasification of Char II and Char IIa. Figure 5 illustrates the kinetic analysis of the gasification of char IIa, which was near identical to that of char II. As presented above, the catalysis of the inherent metallic species is negligible in the gasification of these chars. It was found that the measured $(1 - X)$ was described quantitatively by a function.

$$1 - X = F_1(t) + F_2(t) = C_{10} \exp(-k_1 t) + C_{20} \exp(-k_2 t) \tag{6}$$

The red-colored straight lines indicate $F_1(t)$ and $F_2(t)$. The blue-colored line presents the difference between the measured

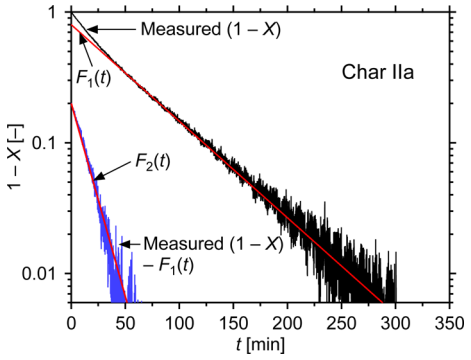

Figure 5. Illustration of the kinetic analysis of the steam gasification of char IIa assuming a kinetic model represented by eqs 6 and 7

$(1 - X)$ and $F_1(t)$ that corresponds to $F_2(t)$. Equation 6 is derived from a rate equation.

$$\frac{dX}{dt} = C_{10}k_1(1 - x_1) + C_{20}k_2(1 - x_2) \tag{7}$$

$$C_{10} + C_{20} = 1, \quad 0 \le x_1 \le 1, \quad 0 \le x_2 \le 1$$

A simple interpretation of eq 7 is that char IIa and char II consist of two components (C1 and C2) reacting with steam following the non-catalytic first-order kinetics with different rate constants, k_1 and k_2, respectively. C_{10} and C_{20} are the initial mass fractions of C1 and C2, respectively. The analysis shows $C_{10} = 0.80$, $C_{20} = 0.20$, $k_1 = 0.017$ min^{-1}, and $k_2 = 0.068$ min^{-1}. The presence of two different carbonaceous components has not been evidenced, but it is consistent with previous studies[53,54] that investigated the structural evolution of char during gasification by Fourier transform (FT)-Raman spectroscopy. Both studies showed that the char carbons with different types were gasified at different rates. As recently reported by the present authors,[17] the solids from 250 °C HTT of different types of biomass solids consisted mainly of lignin and transformed carbohydrates (from cellulose and hemicellulose). It was then speculated that char II and char IIa consisted of carbonaceous materials that were derived from different origins, lignin and others.

An equation with the same type of function as eq 6 can be derived by another kinetic model that considers the progress of non-catalytic gasification and AAEM-catalyzed gasification in parallel.[47,48] The rate of gasification is expressed by

$$\frac{dX}{dt} = k_{nc}(1 - X) + k_{c0} \exp(-k_{loss} t) \tag{8}$$

where k_{nc}, k_{c0}, and k_{loss} are the rate constants for the non-catalytic gasification that has the same meaning as $k_{app,first}$ of eq 4, the AAEM-catalyzed gasification with the same meaning as $k_{app,zeroth}$ of eq 5, and the loss of catalytic activity, respectively. The integration of X with respect to t gives

$$1 - X = \left(\frac{k_{c0}}{k_{loss} - k_{nc}}\right)\exp(-k_{loss} t) + \left(1 - \frac{k_{c0}}{k_{loss} - k_{nc}}\right) \exp(-k_{nc} t) \tag{9}$$

The terms, $(k_{c0}/(k_{loss} - k_{nc}))$, $(1 - (k_{c0}/(k_{loss} - k_{nc})))$, k_{loss}, and k_{nc} correspond to C_{20}, C_{10}, k_1, and k_2 of eq 6, respectively. A particular feature of this parallel reaction model is the assumption of deactivation of the catalyst (i.e., AAEM species) in an exponential manner with time. However, as shown by the

dx.doi.org/10.1021/ef501898h | Energy Fuels 2014, 28, 7133−7139

kinetics of gasification of char I, the deactivation of catalyst, even if present, was implausible. Thus, with knowledge from the present and previous studies, eqs 6 and 7 are reasonable in describing the measured kinetics of gasification of char IIa and char II.

The relationship between the gasification kinetics and specific surface area for char II and char IIa is considered again introducing the following assumptions: (1) Each char consists of two components with different reactivities. (2) Both of the components are gasified following first-order kinetics.

The progress of the first-order reaction means that the oxidizing agent, steam, could diffuse to everywhere in the gasifying char particle and reach active sites, regardless of the char conversion.[32] Both of the rate constants, k_1 and k_2, were steady until complete gasification of C1 and C2, respectively. This was validated by the agreement of experimental data of Figure 5 with the kinetic analysis using eqs 6 and 7. However, S_{BET} increased monotonously from 400−500 to 2300 m^2/g. It is thus reasonable to recognize that the increase in S_{BET} is a result of the progress of gasification, but S_{BET} influences neither k_1 nor k_2. In other words, S_{BET} is not a kinetic factor.

The specific surface areas of char II and char IIa at some different X (0, 0.48, 0.55, and 0.81) were also measured with another adsorbate, CO_2. The results are shown in Figure 6. The

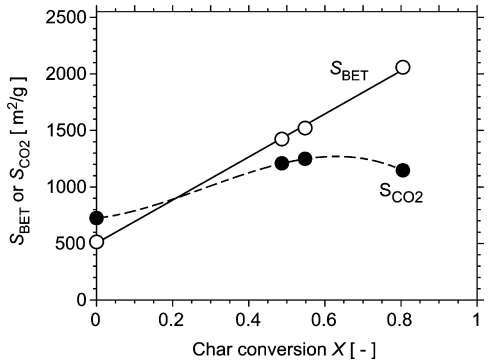

Figure 6. Changes in S_{BET} and S_{CO_2} with X for the gasification of char II and char IIa. The data points at X = 0.48 are those for char IIa, and the others are those for char II.

specific surface area measured with CO_2, S_{CO_2}, in fact varies differently from S_{BET}. There is, however, no basis for that because S_{CO_2} is a kinetic factor for the gasification of char II and char IIa. S_{CO_2} is slightly greater than S_{BET} at X = 0, and this is because some of the pores were ultramicropores that were inaccessible to N_2. The chars at higher X have S_{BET} greater than S_{CO_2}, which is explained by the formation of mesopores that had no contribution to S_{CO_2}. There seems to be a maximum of S_{CO_2}. This indicates that the consumption of ultramicropores was probably associated with the formation of greater pores that contributed to S_{BET} but not to S_{CO_2}.

3.4. Role of Catalyst on the Pore Development. The steam gasification increased S_{BET} of char II and char IIa to ca. 2300 m^2/g. Such extensive surface area development is consistent with the recent report by the authors on the non-catalytic steam reforming of biomass chars.[32] It was then speculated that the non-catalytic steam gasification has a particular feature of producing high surface area char. It was also suspected that the AAEM-catalyzed gasification inhibited the surface area development. Char IIa was loaded with K to prepare char IIa-K1 and char IIa-K2 and subjected to the steam gasification. The results are shown in Figure 7.

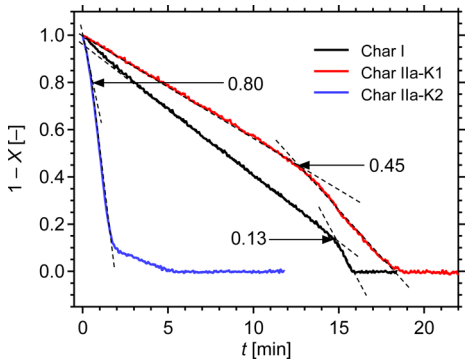

Figure 7. $(1 - X)$ for the gasification of char IIa-K1, char IIa-K2, and char I as functions of t.

Figure 7 shows time-dependent changes in $(1 - X)$ on a decimal scale. The $(1 - X)$ versus t profile for char IIa-K1 is a typical profile for AAEM-catalyzed gasification. The gasification follows zeroth-order kinetics with a LSL at $(1 - X) \approx 0.45$, which is graphically determined. Char IIa-K1 is gasified more slowly than char I. This suggests substantial catalytic contribution of the inherent metals, Ca in particular, to the gasification of char I and probably the difference in the reactivities of the carbonaceous portion of the two chars prepared from the raw cedar and the hydrothermally treated cedar. The gasification of char IIa-K2 is very fast, but its trend is the same as that for char IIa-K1 in a qualitative sense. Although not clear in the figure, a LSL at $(1 - X) \approx 0.80$ was determined. The occurrence of LSL at an earlier stage of gasification at higher K loading is reasonable. The apparent slowdown of the mass release at $t \approx 2$ min is not due to that of the gasification but to the evaporation of K species as KOH.[55] Thus, char IIa-K2 was gasified completely within 2 min.

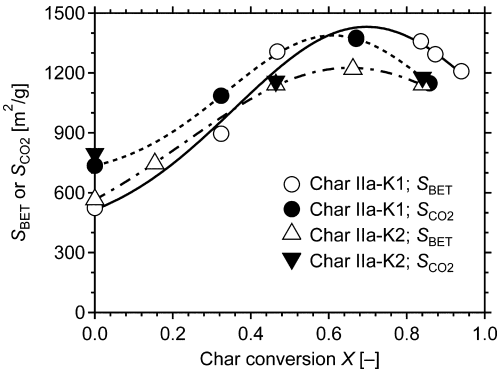

Figure 8. Changes in S_{BET} and S_{CO_2} with the progress of gasification of char IIa-K1 and char IIa-K2.

Figure 8 exhibits the changes in S_{BET} and S_{CO_2} with the progress of gasification of char IIa-K1 and char IIa-K2. The partially gasified char samples were washed with water repeatedly for removing K and dried prior to the analysis. Three important trends are found in this figure. First, S_{BET}

dx.doi.org/10.1021/ef501898h | Energy Fuels 2014, 28, 7133−7139

values for both chars are clearly lower than those for char II and char IIa. The catalysis of K seems to suppress the surface area development. The suppression is more significant at a higher K concentration. Second, S_{BET} and S_{CO_2} are similar to each other. Such similarity suggests that the K-catalyzed gasification created mainly micropores with sizes in a limited range, which contributed equally to S_{BET} and S_{CO_2}.

Third, both S_{BET} and S_{CO_2} change along with X through maxima. The decreases in both S_{BET} and S_{CO_2} at $X >$ ca. 0.7 are ascribed to the loss of micropores with neither their coalescence nor growth to mesopores that contributed solely to S_{BET}. Such behavior of micropores was primarily due to the K catalyst being dispersed in the char matrix maintaining its sizes well below 1.5 nm, which is the upper limit of the width of pores contributing to S_{CO_2}. It was also suggested that close placement of the catalytic K species rapidly eliminated carbon in their vicinities, inhibiting the coalescence and growth to mesopores. Selective formation and development of micropores were reported during chemical activation of biomass-derived chars with alkali salts, such as K_2CO_3 and KOH.[56,57] The third trend, i.e., the changes in S_{BET} and S_{CO_2} with X through maxima, had no direct correspondence with the zeroth-order kinetics of gasification. Thus, neither S_{BET} nor S_{CO_2} is a factor controlling the rate of the catalytic gasification.

4. CONCLUSION

This study investigated the kinetics and mechanism of steam gasification of the chars from the pyrolysis of the original cedar and hydrothermally treated cedar. The following conclusions have been drawn for the gasification within the ranges of the experimental conditions: (1) Char II consists of two carbonaceous components that have different reactivities with steam, which undergo the gasification obeying first-order kinetics over the entire range of X. AAEM species retained in char II have no or very little catalytic activities, and therefore, the acid washing of char II hardly changes the kinetics. (2) The gasification of char II is much slower than that of char I, because of the absence of the catalyst in the former char. (3) S_{BET} of char II increased monotonously and in a linear manner with X and reaches ca. 2300 m^2/g at $X \approx 0.9$. The change in S_{BET} is a result from the gasification but not a kinetic factor. (4) Char I and K-loaded char IIa are gasified following the zeroth-order kinetics because of the catalysis of highly dispersed inherent AAEM species or extraneous K. The catalysis suppresses the development of S_{BET} by inhibiting the formation of mesopores from micropores. (5) Both S_{BET} and S_{CO_2} change via maxima during the K-catalyzed gasification, but neither of these changes is a factor determining the rate of gasification.

AUTHOR INFORMATION

Corresponding Author

*Telephone: +81-92-583-7796. Fax: +81-92-583-7793. E-mail: junichiro_hayashi@cm.kyushu-u.ac.jp.

Notes

The authors declare no competing financial interest.

ACKNOWLEDGMENTS

Lei Bai expresses personal gratitude to Kyushu University for the Friendship Scholarship provided during his participation in this research work. This work was supported by Japan Society for The Promotion of Science (JSPS) for Grant-in-Aid for Scientific Research A (Grant Number 26249120).

REFERENCES

(1) Liu, C.; Wyman, C. E. *Bioresour. Technol.* **2005**, *96*, 1978−1985.
(2) Mosier, N.; Hendrickson, R.; Ho, N.; Sedlak, M.; Ladisch, M. R. *Bioresour. Technol.* **2005**, *96*, 1986−1993.
(3) Mosier, N.; Wyman, C.; Dale, B.; Elander, R.; Lee, Y. Y.; Holtzapple, M.; Ladisch, M. *Bioresour. Technol.* **2005**, *96*, 673−686.
(4) Hendriks, A. T. W. M.; Zeeman, G. *Bioresour. Technol.* **2009**, *100*, 10−18.
(5) Yu, Y.; Lou, X.; Wu, H. *Energy Fuels* **2008**, *22*, 46−60.
(6) Kruse, A.; Maniam, P.; Spieler, F. *Ind. Eng. Chem. Res.* **2007**, *46*, 87−96.
(7) Kruse, A.; Gawlik, A. *Ind. Eng. Chem. Res.* **2003**, *42*, 267−279.
(8) Antal, M. J.; Mok, W. S. L. *Carbohydr. Res.* **1990**, *199*, 91−109.
(9) Kabyemela, B. M.; Adschiri, T.; Malaluan, R. M.; Arai, K. *Ind. Eng. Chem. Res.* **1997**, *36*, 1552−1558.
(10) Srokol, Z.; Bouche, A. G.; Estrik, A. V.; Strik, R. C. J.; Maschmeyer, T.; Peters, J. A. *Carbohydr. Res.* **2004**, *339*, 1717−1726.
(11) Asghari, F. S.; Yoshida, H. *Ind. Eng. Chem. Res.* **2006**, *45*, 2163−2173.
(12) Karagöz, S.; Bhaskar, T.; Muto, A.; Sakata, Y. *Fuel* **2005**, *84*, 875−884.
(13) Liu, A.; Park, Y. K.; Huang, Z.; Wang, B.; Ankumah, R. O.; Biswas, P. K. *Energy Fuels* **2006**, *20*, 446−454.
(14) Mursito, A. T.; Sakaki, K.; Hirajima, T. *Fuel* **2010**, *89*, 635−641.
(15) Iryania, D. A.; Kumagai, S.; Nonaka, M.; Sasaki, K.; Hirajima, T. *Procedia Earth Planet. Sci.* **2013**, *6*, 441−447.
(16) Iryania, D. A.; Kumagai, S.; Nonaka, M.; Nagashima, Y.; Sasaki, K.; Hirajima, T. *Int. J. Green Energy* **2014**, *11*, 577−588.
(17) Kudo, S.; Mori, A.; Soejima, R.; Karnowo; Nomura, S.; Dohi, Y.; Norinaga, K.; Hayashi, J.-i. *ISIJ Int.* **2014**, in press.
(18) Mori, A.; Yuniati, M. D.; Mursito, A. T.; Kudo, S.; Norinaga, K.; Nonaka, M.; Hirajima, T.; Kim, H.-S.; Hayashi, J.-i. *Energy Fuels* **2013**, *27*, 6607−6616.
(19) Mojtahedi, W.; Backman, R. *J. Inst. Energy* **1989**, *62*, 189−196.
(20) Dayton, D. C.; French, R. J.; Milne, T. A. *Energy Fuels* **1995**, *8*, 855−865.
(21) Olsson, J. G.; Jäglid, U.; Pettersson, J. B. C.; Hald, P. *Energy Fuels* **1997**, *11*, 779−784.
(22) Dayton, D. C.; Jenkins, B. M.; Turn, S. Q.; Bakker, R. R.; Williams, R. B.; Belle-Oudry, D.; Hill, L. M. *Energy Fuels* **1999**, *13*, 860−870.
(23) Jensen, P. A.; Frandsen, F. J.; Dam-Johansen, K.; Sander, B. *Energy Fuels* **2000**, *14*, 1280−1285.
(24) Knudsen, J. N.; Jensen, P. A.; Dam-Johansen, K. *Energy Fuels* **2004**, *18*, 1385−1399.
(25) Öhman, M.; Pommer, L.; Nordin, A. *Energy Fuels* **2005**, *19*, 1742−1748.
(26) Raveendran, K.; Ganesh, A. *Fuel* **1998**, *77*, 769−781.
(27) Zolin, A.; Jensen, A.; Jensen, P. A.; Frandsen, F.; Dam-Johansen, K. *Energy Fuels* **2001**, *15*, 1110−1122.
(28) Keown, D.; Favas, G.; Hayashi, J.-i.; Li, C.-Z. *Bioresour. Technol.* **2005**, *96*, 1570−1577.
(29) Kajita, M.; Kimura, T.; Norinaga, K.; Li, C.-Z.; Hayashi, J.-i. *Energy Fuels* **2010**, *24*, 108−116.
(30) Sueyasu, T.; Oike, T.; Mori, A.; Kudo, S.; Norinaga, K.; Hayashi, J.-i. *Energy Fuels* **2012**, *26*, 199−208.
(31) Hosokai, S.; Norinaga, K.; Kimura, T.; Nakano, M.; Li, C.-Z.; Hayashi, J.-i. *Energy Fuels* **2011**, *25*, 5387−93.
(32) Kudo, S.; Hachiyama, Y.; Kim, H.-S.; Norinaga, K.; Hayashi, J.-i. *Energy Fuels* **2014**, *28*, 5902−5908.
(33) Sohn, H. Y.; Szekely, J. *Chem. Eng. Sci.* **1972**, *27*, 763−778.
(34) Bhatia, S. K.; Perlmutter, D. D. *AIChE J.* **1980**, *26*, 379−386.
(35) Adschiri, T.; Furusawa, T. *Fuel* **1986**, *65*, 927−931.
(36) Yip, K.; Tian, F.; Hayashi, J.-i.; Wu, H. *Energy Fuels* **2009**, *24*, 173−181.

(37) Kajitani, S.; Suzuki, N.; Ashizawa, M.; Hara, S. *Fuel* **2006**, *85*, 163−169.
(38) Seo, D. K.; Lee, S. K.; Kang, M. W.; Hwang, J.; Yu, T.-U. *Biomass Bioenergy* **2010**, *34*, 1946−1953.
(39) Jenkins, R. G.; Nandi, S. P.; Walker, P. L., Jr. *Fuel* **1973**, *52*, 288−293.
(40) Adschiri, T.; Nozaki, T.; Furusawa, T.; Zi-bin, Z. *AIChE J.* **1991**, *37*, 897−904.
(41) Feng, B.; Bhatia, S. K. *Carbon* **2003**, *41*, 507−523.
(42) Cetin, E.; Gupta, R.; Moghtaderi, B. *Fuel* **2005**, *84*, 1328−1334.
(43) Fu, P.; Hu, S.; Xiang, J.; Yi, W.; Bai, X.; Sun, L.; Su, S. *Bioresour. Technol.* **2012**, *114*, 691−697.
(44) Lin, S.; Zhu, Z.; Hirato, M.; Ninomiya, Y.; Horio, M. *Kagaku Kogaku Ronbunshu* **1993**, *19*, 325−332.
(45) Kajitani, S.; Hara, S.; Matsuda, H. *Fuel* **2002**, *81*, 539−546.
(46) Li, C. Z.; Sathe, C.; Kershaw, J. R.; Pang, Y. *Fuel* **2000**, *79* (3−4), 427−438.
(47) Bayarsaikhan, B.; Hayashi, J.-i.; Shimada, T.; Sathe, C.; Li, C.-Z.; Tsutsumi, A.; Chiba, T. *Fuel* **2005**, *84*, 1612−1621.
(48) Kitsuka, T.; Bayarsaikhan, B.; Sonoyama, N.; Hosokai, S.; Li, C.-Z.; Norinaga, K.; Hayashi, J.-i. *Energy Fuels* **2007**, *21*, 387−394.
(49) Wu, H.; Hayashi, J.-i.; Chiba, T.; Takarada, T.; Li, C.-Z. *Fuel* **2004**, *83*, 23−30.
(50) Chen, S. G.; Yang, R. T. *J. Catal.* **1992**, *138*, 12−23.
(51) Suzuki, T.; Ohme, H.; Watanabe, Y. *Energy Fuels* **1992**, *6*, 343−351.
(52) Chen, S. G.; Yang, R. T. *Energy Fuels* **1997**, *11*, 421−427.
(53) Keown, D. M.; Li, X.; Hayashi, J.-i.; Li, C.-Z. *Fuel. Process. Technol.* **2008**, *89*, 1429−1435.
(54) Yip, K.; Ng, E.; Li, C.-Z.; Hayashi, J.-i.; Wu, H. *Proc. Combust. Inst.* **2011**, *33*, 1755−1762.
(55) Sueyasu, T.; Oike, T.; Mori, A.; Kudo, S.; Norinaga, K.; Hayashi, J.-i. *Energy Fuels* **2012**, *26*, 199−208.
(56) Hayashi, J.; Kazehaya, A.; Muroyama, K.; Watkinson, A. P. *Carbon* **2000**, *38*, 1873−1878.
(57) Hayashi, J.; Horikawa, T.; Takeda, I.; Muroyama, K.; Ani, F. N. *Carbon* **2002**, *40*, 2381−2386.